Journal of Power Sources 263 (2014) 90–97

Contents lists available at ScienceDirect

Journal of Power Sources

journal homepage: www.elsevier.com/locate/jpowsour

New insights into the $GdBaCo_2O_{5+\delta}$ material: Crystal structure, electrical and electrochemical properties

Daniel Muñoz-Gil [a], Domingo Pérez-Coll [b], Juan Peña-Martínez [c], Susana Garcia-Martín [a,*]

[a] Departamento de Química Inorgánica I, Facultad de Ciencias Químicas, Universidad Complutense, 28040 Madrid, Spain
[b] Instituto de Cerámica y Vidrio, CSIC, Cantoblanco, 28049 Madrid, Spain
[c] Departamento de Didáctica de las Ciencias Experimentales, Facultad de Educación, Universidad Complutense, 28040 Madrid, Spain

HIGHLIGHTS

- Different crystal structure is determined for $GdBaCo_2O_{5+\delta}$ depending on the oxygen content.
- A new superstructure with $a_p \times 3a_p \times 2a_p$ unit cell is observed for δ values close to 0.33.
- A total polarization resistance of 0.04 Ω cm^2 is achieved at 650 °C for $GdBaCo_2O_{5+\delta}$ prepared in Ar.

ARTICLE INFO

Article history:
Received 17 January 2014
Received in revised form
19 March 2014
Accepted 7 April 2014
Available online 13 April 2014

Keywords:
Intermediate temperature solid oxide fuel cells
GBCO
Perovskite structure
Electrical properties

ABSTRACT

Selected area electron diffraction (SAED) and high resolution transmission electron microscopy (HRTEM) studies reveal that the crystal structure and microstructure of $GdBaCo_2O_{5+\delta}$ are highly influenced by the oxygen stoichiometry. In addition to layered-type ordering of the Ba and Gd atoms along the *c*-direction of the structure and location of anion vacancies within the $(GdO)_x$ planes giving a $a_p \times a_p \times 2a_p$ unit cell, two different perovskite related superstructures are observed. A superstructure with $a_p \times 3a_p \times 2a_p$ unit cell, probably due to extra ordering of the anion vacancies within the $(GdO)_x$ planes is formed for δ values close to 0.33 and a superstructure with $\sqrt{2}a_p \times \sqrt{2}b_p \times 2a_p$ unit cell associated to tilting of the CoO_6 octahedra appears for the compound with δ values close to 1. Domain formation with perpendicular orientations of the unit cell occurs in crystals with orthorhombic symmetry of the structure. Physical properties of the aforementioned material, which is well known as a potential candidate of cathode for intermediate temperature solid oxide fuel cells, are likely to be strongly affected by its oxygen stoichiometry and therefore by its crystal structure and microstructure.

1. Introduction

There is a growing interest in the study of perovskites of general formula $A_{1-x}A'_xM_{1-y}M'_yO_{3-\delta}$ (A = lanthanide atom, A′ = alkali earth atom and M, M′ = transition metal atom) as electrodes in solid oxide fuel cells (SOFCs) [1,2]. In particular, A-site ordered cobaltites $AA'Co_2O_{5+\delta}$, also called layered-type perovskites, are promising candidates as cathodes for intermediate temperature solid oxide fuel cells (IT-SOFCs) due to their excellent electronic and ionic conductivity [3–7]. The high oxygen mobility in these perovskites seems to be related to the A-cation ordering [8,9].

$GdBaCo_2O_{5+\delta}$ is a layered-type perovskite. It shows a wide range of oxygen non-stoichiometry and its attractive physical and structural properties depend on the oxygen content. The oxygen content and therefore the crystal structure and properties of this oxide depend on the synthesis conditions. In this sense, $GdBaCo_2O_{5+\delta}$ with δ values close to 0 has been prepared in Ar atmosphere and δ values higher than 0.4 are always determined for samples prepared in air with a slow cooling or annealed in oxygen flow. The crystal structure of $GdBaCo_2O_{5+\delta}$ derives from the 112-type structure with $a_p \times a_p \times 2a_p$ unit cell (a_p refers to the lattice parameter of the cubic perovskite) [10]. In this structure with $\delta = 0$, Gd and Ba are ordered into layers along the *c* axis and all the Co atoms are coordinated by O in squared pyramids. The oxygen non-stoichiometry is accommodated within the $(GdO)_x$ planes in such a way that different supercells have been proposed in the literature depending on the oxygen content and the ordering of the anion vacancies (or the oxygen anions) in those planes [11–15]. $GdBaCo_2O_{5.5}$ has a 122-type structure ($a_p \times 2a_p \times 2a_p$ unit cell) due to extra ordering of the oxygen anions in the $(GdO)_x$ planes [13,14].

* Corresponding author. Tel.: +34 913944214; fax: +34 913944352.
E-mail address: sgmartin@quim.ucm.es (S. Garcia-Martín).

http://dx.doi.org/10.1016/j.jpowsour.2014.04.019
0378-7753/

This 122-type structure has been proposed for all the $GdBaCo_2O_{5+\delta}$ oxides with $\delta > 0.4$ [11–15]. Besides, a crystal structure with $3a_p \times 3a_p \times 2a_p$ unit cell has recently been reported for a $GdBaCo_2O_{5+\delta}$ single crystal with $\delta \sim 0.38$ [16]. Magnetic and electric properties of $GdBaCo_2O_{5+\delta}$ are also highly sensitive to the oxygen non-stoichiometry [11,15].

The electrochemical behaviour of $GdBaCo_2O_{5+\delta}$ for IT-SOFC applications was reported for the first time in 2006 [3]. This oxide was studied as cathode material in a symmetrical cell configuration using $Ce_{0.8}Gd_{0.2}O_{2-\delta}$ as electrolyte, obtaining area-specific resistance (ASR) as low as 0.53 Ω cm^2 at 645 °C. Optimization of the preparation of the cells improves the electrochemical performance, decreasing the ASR down to values of ~0.3 Ω cm^2 at 650 °C and therefore corroborating that this material might be an excellent cathode for IT-SOFCs [4]. However, poor long-term stability of this cathode material when exposing to ambient air, in particular reaction with CO_2 like those reported in other Ba-containing IT-SOFC cathode materials, [17,18] may be a potential drawback to overcome. On the contrary, studies about GBCO in different CO_2 atmospheres indicate that this compound does not suffer phase degradation in atmospheres with CO_2 concentration lower than 600 ppm, and operation temperatures between 500 and 700 °C [19].

The crystal structure of $GdBaCo_2O_{5+\delta}$, in particular the $(GdO)_x$ planes, has a significant influence on its ion conducting properties. Molecular Dynamics studies indicate that oxygen diffusion occurs only in the $(GdO)_x$ planes and cation disorder of the Gd/Ba sublattice results in a reduction of the oxygen diffusion and the appearance of diffusion also along the *c* axis of the structure [20]. These results are in agreement with those reported by Taskin et al., [8,9] which suggest that oxygen diffusion is significantly higher in layered-type perovskites in comparison with the corresponding cation disordered oxides. In fact, recent experimental results confirm oxygen anisotropy diffusion in $PrBaCo_2O_{5+\delta}$ [21]. Ordering of the anion vacancies within the $(GdO)_x$ planes, in combination with the oxygen non-stoichiometry must affect the oxygen diffusion properties in this material and therefore its capability as cathode in SOFCs. In this context, we present in this paper a new contribution to the general understanding of the relations between oxygen non-stoichiometry, crystal structure and electrical and electrochemical properties of $GdBaCo_2O_{5+\delta}$. We have found that the synthesis conditions for preparing this material have a great impact not only on its oxygen content and crystal structure but also in its electrical and electrochemical behaviour as cathode in SOFCs.

2. Experimental

$GdBaCo_2O_{5+\delta}$ (GBCO) has been prepared by solid state reaction using Gd_2O_3 (Sigma Aldrich, 99.99%), $BaCO_3$ (Sigma Aldrich, 99.99%) and Co_2O_3 (Sigma Aldrich, 99.99%). Gd_2O_3 was heated at 900 °C prior to weighing. Stoichiometric amounts of the starting compounds were ground together and heated at 1000 °C for 12 h for decarbonation in air or under a gas flow of Argon (purity ≥ 99.999). Afterwards, the samples were again grounded, pelleted and then fired at 1200 °C in air or under Ar atmosphere. Samples prepared in Ar were slowly cooled in the furnace at 2 °C min^{-1}, whereas samples prepared in air were either slowly cooled in the furnace at 2 °C min^{-1} or quenched to room temperature on a brass plate.

Oxygen content of the samples has been determined by redox titration using $K_2Cr_2O_7$ [22] and thermogravimetric analysis (TGA) at 900 °C under $N_2 + H_2$ (% $H_2 < 5.7\%$) gas flow in an SDT Q600 thermogravimetric analyser. The extent of the decomposition was checked by XRD. After reduction of the samples, only Gd_2O_3, BaO and Co were detected in the PXRD patterns. TGA have also been carried out in air and in oxygen to evaluate oxygen stoichiometry stability of the samples from 25 °C to 900 °C.

Crystalline phase identification was carried out by powder X-ray diffraction (PXRD) using a PANalytical X'PERT PRO MPD diffractometer with Cu Kα1 radiation and X'PERT PEAPD software. The patterns were taken at step mode with a step size equal to 0.02 (2θ degrees) and time per step equal to 10 s.

Selected area electron diffraction (SAED) and high resolution transmission electron microscopy (HRTEM) studies have been performed with a JEOL JEM 3000F microscope operating at 300 kV (double tilt (±20°) (point resolution 1.7 Å)), fitted with an XEDS microanalysis system (OXFORD INCA). The atomic ratio of the metals has been determined by X-ray energy dispersive spectroscopy (XEDS) analyses finding good agreement between analytical and nominal composition in all the crystals. For transmission electron microscopy the samples were ground in *n*-butyl alcohol and ultrasonically dispersed. A few drops of the resulting suspension were deposited in a carbon-coated grid.

Total electrical conductivity of dense samples was determined by a d.c. four-probe method in air, O_2 and N_2 atmospheres. For this purpose two Pt wires were attached with Au paste (Heraeus C5754) to the external surfaces of rectangular bars in order to produce a homogeneous current flux through the sample by means of a potentiostat/galvanostat equipment in galvanostatic mode (Autolab PGSTAT302N). Another pair of Pt wires was internally attached to the sample to record the voltage drop associated to the volumetric resistance between the inner wires. Samples were equilibrated at 950 °C for 12 h in the corresponding atmosphere before the electrical study was performed by decreasing temperature from 950 to 200 °C with a cooling rate of 5 °C min^{-1} in steps of 50 °C. Experimental resistances were obtained by the slope of *V–I* curve in the current range of 50–500 mA.

Area specific resistance (ASR) associated to the electrode polarisation process at different temperatures has been determined by AC impedance spectroscopy on symmetrical two-electrode cells. The impedance measurements were carried out using a frequency response analyzer Solartron 1255A with a dielectric interface 1296. Measurements were performed in air on heating and cooling cycles between 500 °C and 700 °C, in a frequency range of 0.1 Hz–1 MHz and an excitation voltage of 50 mV. Electrolyte pellets of 10 mm diameter and 1.2 mm thickness of commercial $Ce_{0.9}Gd_{0.1}O_{2-\delta}$ (CGO) powder (Fuel Cells Materials) were prepared by pressing the powder at 250 MPa and sintering in air at 1400 °C for 12 h. A slurry prepared by $GdBaCo_2O_{5+\delta}$:CGO composites (70:30 wt %) with a commercial organic vehicle (Decoflux™) was deposited onto both surfaces of the CGO electrolyte and then fired at 900 °C for 3 h in air (heating/cooling rate of 2.5 °C min^{-1}). Silver paste and mesh were used as current collectors on both sides of the pellets. The impedance spectra were fitted to equivalent circuits using the Zview software [23].

3. Results and discussion

Fig. 1a shows the PXRD patterns at room temperature of $GdBaCo_2O_{5+\delta}$ samples prepared under different conditions: in air with slow cooling (GBCO Air-SC), in air and quenched to room temperature (GBCO-Air-Q) and in Ar flow with slow cooling (GBCO-Ar). Single phase materials were obtained in all cases. The patterns are characteristic of layered-type perovskite showing reflections associated to the cubic perovskite structure (p refers to cubic perovskite) and extra reflections related to lowering of symmetry and ordering of the Ba and Gd cations. Significant differences are observed in the patterns in such a way that the PXRD patterns of the GBCO-Air-Q and GBCO-Ar samples can be indexed using a tetragonal unit cell $a_p \times a_p \times 2a_p$ and the patterns of the GBCO-Air-

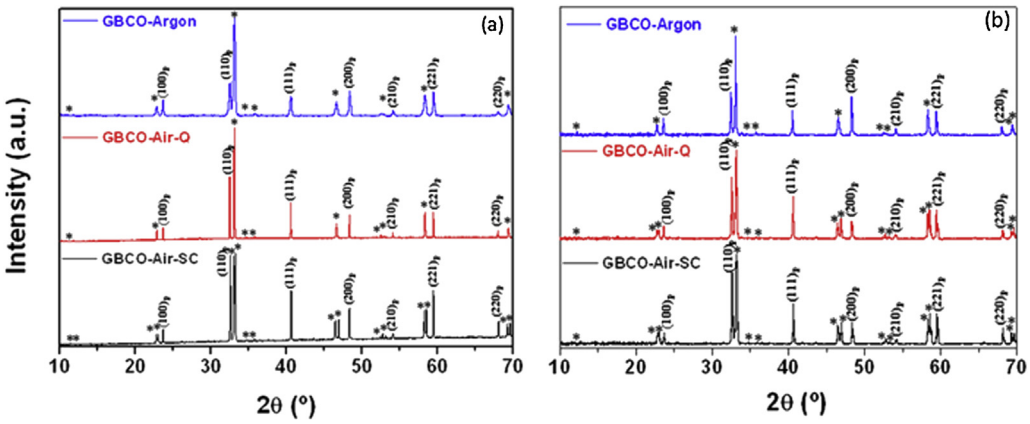

Fig. 1. (a) PXRD patterns of GBCO-Air-SC, GBCO-Air-Q and GBCO-Ar at room temperature. Reflections of cubic perovskite structure are indicated by the corresponding Miller Indices. Extra reflections related to lowering of symmetry and ordering of the Ba and Gd cations are marked by asterisks. (b) PXRD patterns of GBCO-Air-SC, GBCO-Air-Q and GBCO-Ar after the first heating–cooling cycle.

SC using an orthorhombic $a_p \times 2b_p \times 2a_p$ one, as it is deduced from splitting of some reflections.

Table 1 shows the oxygen content of the three $GdBaCo_2O_{5+\delta}$ compounds determined by redox titration and by TGA. Oxygen contents with $\delta < 0.5$ are obtained if the material is prepared in Ar or in air with quenching to room temperature. On the contrary, $\delta > 0.5$ values are obtained if the samples are prepared in air with slow cooling.

Figs. 2–4 show SAED patterns along different zone axes of crystals of GBCO prepared under different conditions. The patterns have been indexed according to the cubic perovskite structure. There are clear differences in the SAED patterns related to differences in the crystal structure of the $GdBaCo_2O_{5+\delta}$. The patterns of the sample prepared in Ar (Fig. 2a–d) show the reflections characteristic of the perovskite structure and extra reflections at $G_p \pm 1/2(001)^*_p$ associated to the layered-type ordering of Ba and Gd along the $[001]_p$ direction, as expected. The unit cell of the crystal structure, deduced from these SAED patterns, is $a_p \times a_p \times 2a_p$, in agreement with the XRD results. When the material is prepared in air with slow cooling, the pattern along the $[010]_p$ zone axis (Fig. 3a) also shows the reflections at $G_p \pm 1/2(001)^*_p$ due to the Ba/Gd ordering and reflections at $G_p \pm 1/2(010)^*_p$, which could indicate doubling of at least two of the main lattice parameters (a_p) of the crystal structure. In addition to them, the patterns in Fig. 3 show ½$(oeo)_p$ reflections associated to in-phase tilting of the octahedral network [24]. This is in good agreement with the oxygen content of the compound (δ values close to 1), which indicates that the Co atoms are mainly in octahedral coordination, in contrast to what occurs in the compounds with oxygen contents with $\delta < 0.5$, in which the Co atoms are mainly in squared-pyramid coordination. Tilting of the MO_6 octahedra for optimizing the A–O bond distances is one of the main distortions occurring in perovskite-type oxides. The patterns of the sample prepared in air with quenching to room temperature (Fig. 4a–c) show reflections at $G_p \pm 1/2(001)^*_p$ associated to the layered-type ordering of Ba and Gd along the $[001]_p$ direction and extra reflections at $G_p \pm 1/3(010)^*_p$ characteristic of a modulation of the crystal structure along the $[010]_p$ direction. This modulation of the crystal structure is probably associated to ordering of the anion vacancies within the $(GdO)_x$ planes leading to a crystal structure with $a_p \times 3a_p \times 2a_p$ unit cell. However, some crystals of this sample also show reflections at $G_p \pm 1/3(100)^*_p$ (see the pattern in Fig. 4c) indicating the possibility of a new cell of dimensions $3a_p \times 3a_p \times 2a_p$. Similar SAED patterns have previously been reported for $HoBaCo_2O_{5.3}$ [11].

HRTEM images give us complementary information of the local crystal structure. Fig. 2e shows the HRTEM image along the $[-110]_p$ zone axis of a crystal of GBCO-Ar. Contrast differences in agreement with a $2a_p$ periodicity along the $[001]_p$ direction are observed in the image. However, the HRTEM image of the crystal of GBCO-Air-SC along the $[010]_p$ zone axis (Fig. 3c) shows contrast differences indicating a $2a_p$ periodicity along two perpendicular directions. Therefore, the structure has a $\sqrt{2}a_p \times \sqrt{2}b_p \times 2a_p$ unit cell and the crystals are formed by domains of this cell oriented along perpendicular directions. Domain formation due to different orientation of the unit cell is very common in oxides with perovskite structure with tilting of the octahedral network [25,26] and it has previously been observed in $GdBaCo_2O_{5.4}$ [11] but despite this fact, an $a_p \times 2a_p \times 2a_p$ unit cell was ascribed to the crystal structure of this compound. In the HRTEM image of the crystal of the sample GBCO-Air-Q along the $[001]_p$ zone axis (Fig. 4d), contrast differences indicating a $3a_p$ periodicity are clearly seen. Nano-domain formation in the crystal is also observed in this image, which shows the $3a_p$ periodicity along two perpendicular directions in very small areas of the crystal. Therefore, the crystal structure of this compound has an $a_p \times 3a_p \times 2a_p$ unit cell due to layered-type ordering of the Ba and Gd atoms and probably ordering of the anion vacancies within the $(GdO)_x$ planes in nano-domains. Fig. 4e displays a crystal structure representation for $GdBaCo_2O_{5.33}$ in agreement with this ordering model. A unit cell of dimensions $a_p \times 3a_p \times 2a_p$ agrees with an oxygen stoichiometry corresponding to $\delta = 0.33$, very close to the δ value that we obtained in the sample prepared in air and quenched to room temperature (Table 1). However, an ordering corresponding to a $3a_p \times 3a_p \times 2a_p$ unit cell, as it was reported for $HoBaCo_2O_{5.3}$ [11], implies a theoretical $\delta = 0.11$.

Two structural phase transitions (at about 80 °C and 450 °C) in combination with variations of the oxygen content have been reported for $GdBaCo_2O_{5+\delta}$ synthesized in air with a slow cooling [27,28]. Therefore, the material could suffer modifications in both the oxygen content and the structure during electrical and

Table 1
Oxygen contents of $GdBaCo_2O_{5+\delta}$ samples.

Sample	Redox titration	TGA
GBCO-Air-SC	5.8 (1)	5.85
GBCO-Air-Q	5.3 (1)	5.39
GBCO-Argon	5.4 (1)	5.45

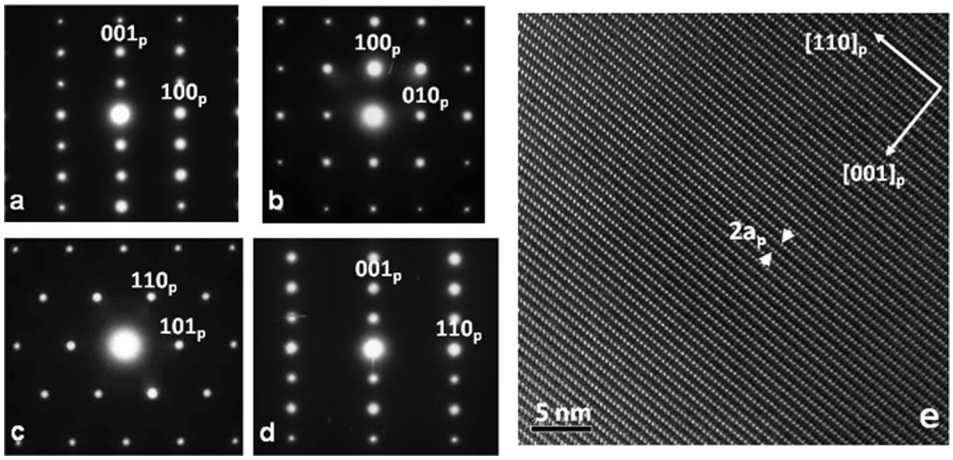

Fig. 2. SAED patterns of a crystal of GBCO-Ar along the $[010]_p$ (a), $[001]_p$ (b), $[-111]_p$ (c) and $[-110]_p$ (d) zone axes. (e) HRTEM image of a crystal of GBCO-Ar along the $[-110]_p$ zone axis.

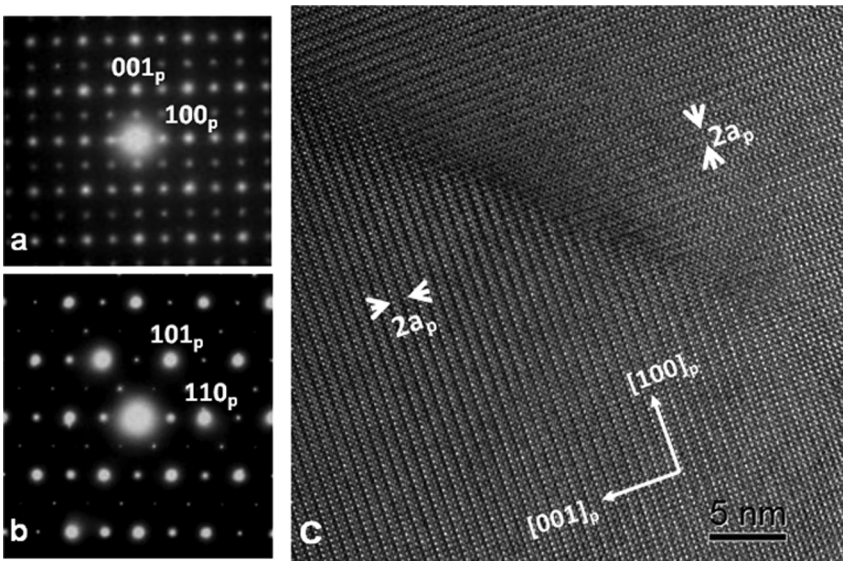

Fig. 3. SAED patterns of a crystal of GBCO-Air-SC along the (a) $[010]_p$ and (b) $[-111]_p$ zone axes. (c) HRTEM image of a crystal of GBCO-Air-SC along the $[010]_p$ zone axis.

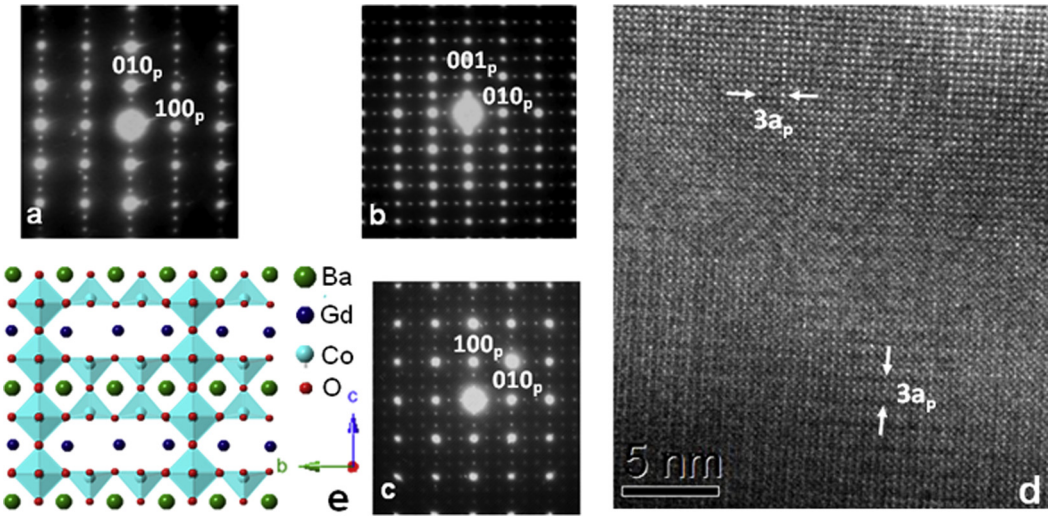

Fig. 4. SAED patterns of a crystal of GBCO-Air-Q along the $[001]_p$ (a) and $[100]_p$ (b) zone axes; SAED pattern (c) and HRTEM image (d) of a crystal of GBCO-Air-Q along the $[001]_p$ zone axis with domain formation. (e) Drawing of the crystal structure of $GdBaCo_2O_{5.33}$ with $a_p \times 3a_p \times 2a_p$ unit cell along the $[100]_p$ zone axis.

electrochemical measurements, which are performed on heating and cooling rates, and even after deposition of the slurry of $GdBaCo_2O_{5+\delta}$:CGO composites on the surfaces of the CGO electrolyte because the cell is fired at 900 °C for 3 h in air and slowly cooled. With the aim of evaluating these possible modifications of the samples during the measurements, we have carried out thermogravimetric analysis, and PXRD, SAED and HRTEM after one heating and cooling cycle from room temperature to 900 °C of the three different samples.

Fig. 5 shows thermogravimetric curves of the three samples. Variation of the oxygen content with temperature of the compounds is also indicated in the graphic representation taking as initial content the one obtained by titration. The mass increase at 200–400 °C upon heating the samples in air is mainly ascribed to oxidation of the compounds because similar results were obtained

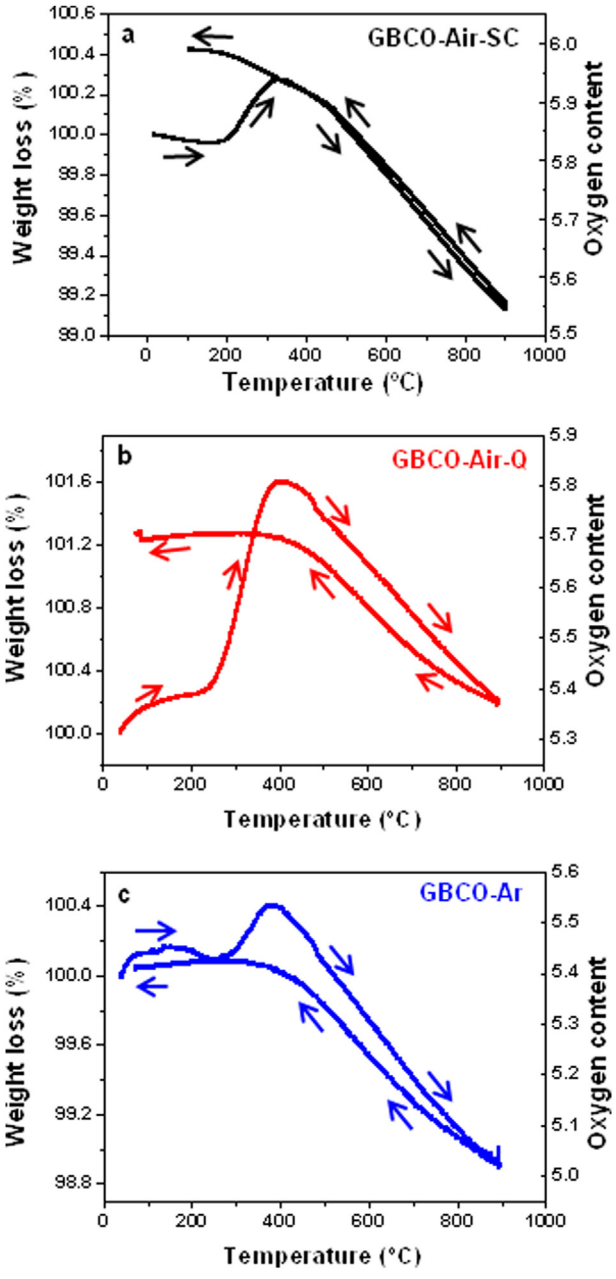

Fig. 5. Thermogravimetric curves in ambient air for (a) GBCO-Air-SC, (b) GBCO-Air-Q and (c) GBCO-Ar. Heating and cooling cycles are indicated by arrows.

when the TGA were performed under oxygen flow. The oxygen content of GBCO-Air-SC and GBCO-Ar slightly increases from room temperature up to about 400 °C. On the contrary, GBCO-Air-Q shows a significant oxygen uptake in this temperature range. Above 400 °C, the three samples have oxygen loss and on cooling they oxidized. The sample prepared in Ar remains with low oxygen contents ($\delta < 0.5$ values) within a heating–cooling cycle while the sample prepared in air with slow cooling always have oxygen contents with $\delta > 0.5$ values. On the contrary, the GBCO-Air-Q sample suffers big changes on the oxygen content during the first heating–cooling cycle. PXRD patterns of the samples after the first heating–cooling cycle (Fig. 1b) indicate that the GBCO-Air-SC and the GBCO-Ar do not modify their crystal structure. However, splitting of reflections is clearly observed in the pattern of the GBCO-Air-Q sample after the first heating–cooling cycle in comparison with the pattern of this sample as prepared. SAED and HRTEM results also show modifications of the crystal structure of the GBCO-Air-Q sample after the first heating–cooling cycle (Fig. 6). The pattern along the $[010]_p$ zone axis shows the reflections at $G_p \pm 1/2(001)^*_p$ due to the Ba/Gd ordering and reflections at $G_p \pm 1/2(010)^*_p$; the corresponding HRTEM image of the crystal shows contrast differences indicating a $2a_p$ periodicity along two perpendicular directions and therefore the crystal is formed by domains with the Ba/Gd ordering perpendicularly oriented. However, reflections associated to tilting of the octahedral network are not observed in the patterns, indicating a structure with $a_p \times b_p \times 2a_p$ unit cell and with values of the a and b lattice parameters very similar. On the contrary, a and b lattice parameters are significantly different in the compound prepared in air with slow cooling. Therefore, it seems that there are two possible orthorhombic crystal structures for $GdBaCo_2O_{5+\delta}$ with $\delta > 0.5$: one is pseudo-tetragonal with $a_p \times b_p \times 2a_p$ unit cell and the other one with $\sqrt{2}a_p \times \sqrt{2}b_p \times 2a_p$ unit cell due to tilting of the octahedra-network in addition to the Ba/Gd ordering for δ values close to 1. It is worth mentioning that the pseudo-tetragonal unit cell is also observed in few crystals of the GBCO-Air-SC sample as prepared probably due to slight differences on the oxygen content of the crystals. In fact, the PXRD patterns in Fig. 1a can be indexed as a phase mixture of crystals with different structure $\sqrt{2}a_p \times \sqrt{2}b_p \times 2a_p$ and $a_p \times b_p \times 2a_p$.

Fig. 7 shows the electrical conductivity of GBCO-Ar as a function of temperature in different atmospheres. A similar trend was obtained for all the samples, with the conductivity increasing with the oxidising character of the gas. This behaviour corresponds to p-type electronic conduction, in which the creation of holes is favoured by the higher oxygen partial pressure as follows:

$$\frac{1}{2}O_2 + V_O^{\cdot\cdot} \leftrightarrow O_O^x + 2h^{\cdot} \quad (1)$$

The results obtained in N_2 show typical semiconductor behaviour in the whole range of temperature. The conductivity increasing with temperature due to the higher mobility of holes and with an activation energy of about $E_a \approx 0.08$ eV. A different behaviour is observed for samples measured under air and O_2 atmospheres. In the lower range of temperature, the results also reveal semiconductor behaviour with values of activation energies as low as ≈0.02 and ≈0.03 eV for O_2 and air atmospheres, respectively. However, for temperatures higher than 400 °C, the conductivity decreases with increasing the temperature, in agreement with some results previously reported in the literature for $GdBaCo_2O_{5+\delta}$ [27,29,30]. This trend can be ascribed to a decrease of p-type carriers when increasing the temperature due to oxygen loss. Note that according to electroneutrality conditions in Eq. (1), an increase in the concentration of oxygen vacancies

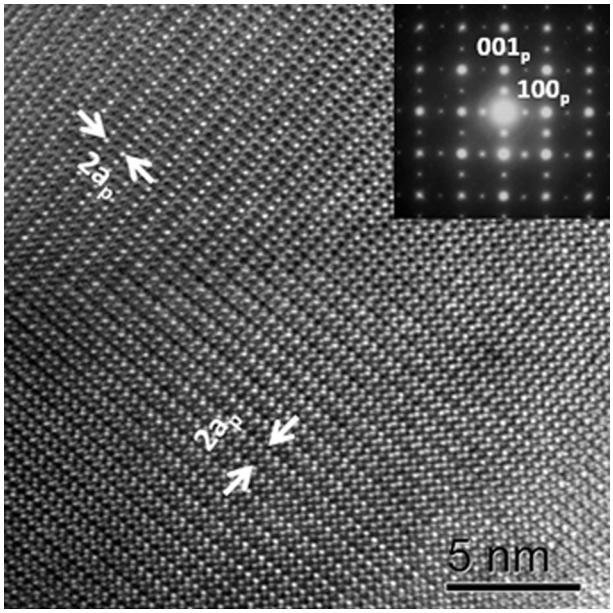

Fig. 6. SAED pattern and HRTEM image along the $[001]_p$ zone axis of a crystal of GBCO-Air-Q after the first heating/cooling cycle.

($[V_O^{\cdot\cdot}]$) should be followed by a decrease in the concentration of holes ($[h^{\cdot}]$).

Fig. 8 shows a comparison of the temperature dependence of conductivity in air for samples prepared under different conditions (GBCO-SC and GBCO-Ar). Although both samples have the same conductivity behaviour as a function of temperature, GBCO-SC shows a significant higher conductivity than GBCO-Ar, which should be ascribed to a higher oxygen content (lower concentration of oxygen vacancies) in the whole range of temperature and therefore to a higher concentration of p-type carriers in order to retain the electroneutrality.

Fig. 9a shows complex impedance diagrams of cells based on GBCO-Air-SC and GBCO-Ar as electrode materials recorded in air at 550 °C. Fig. 9b shows, as example, the complex impedance diagram

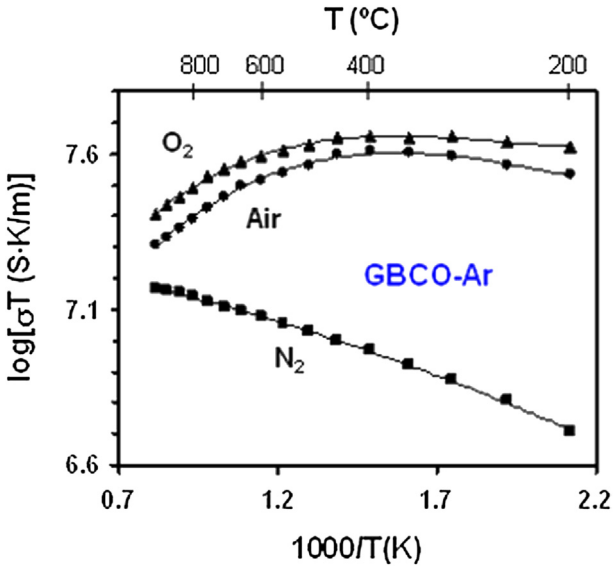

Fig. 7. Arrhenius representation of total conductivity for GBCO-Ar measured in N_2, air and O_2 atmospheres.

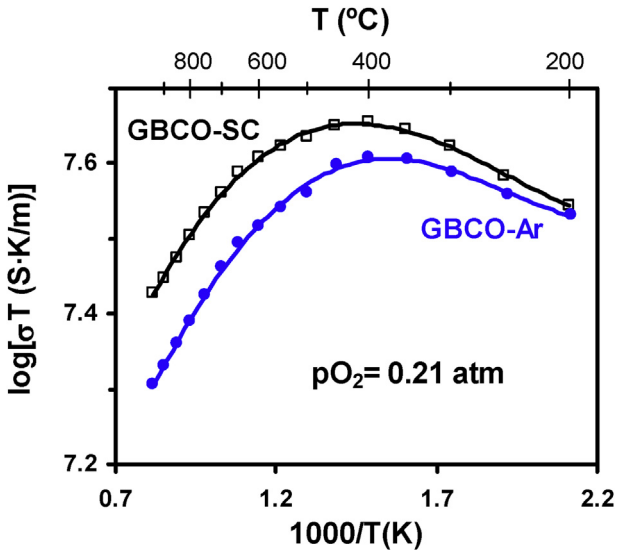

Fig. 8. Temperature dependence of conductivity for GBCO-Air-SC and GBCO-Ar samples in air.

of the cell corresponding to GBCO-Ar at 550 °C fitted using the equivalent circuit indicated in the inset, in which the electrode process displays two major contributions, at intermediate and low frequencies. In order to separate the different contributions, the impedance spectra have been fitted to a series circuit, based on an inductance (L) caused by the electrochemical setup, an ohmic resistance, (Rs) mainly, associated to the total ion transport in the electrolyte and two parallel RQ circuits associated to processes at the electrolyte–electrode interface and at the electrode surface,

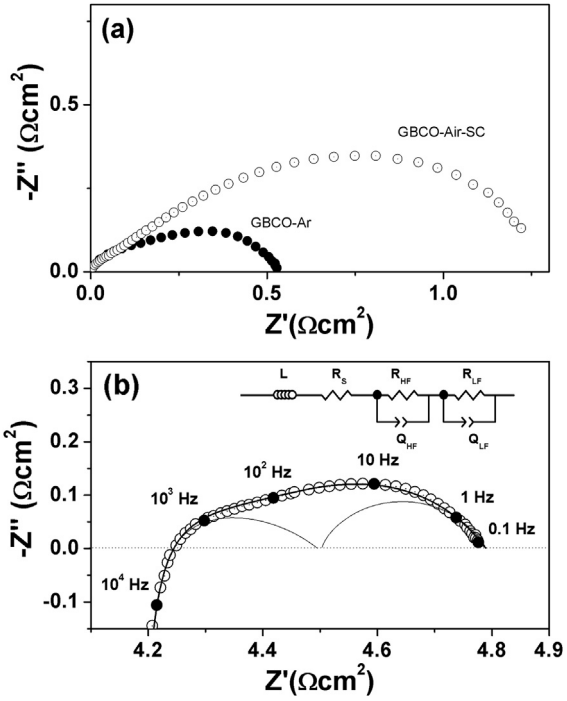

Fig. 9. (a) Impedance spectra for the symmetrical cells of GBCO/CGO at 550 °C in air. Open and closed circles correspond to GBCO-Air-SC and GBCO-Ar respectively. The impedance spectra have been shifted to x-axis origin for comparison. (b) Impedance spectrum for GBCO-Ar fitted by the equivalent circuit represented in the inset. The solid line is the fitting result using the equivalent circuit.

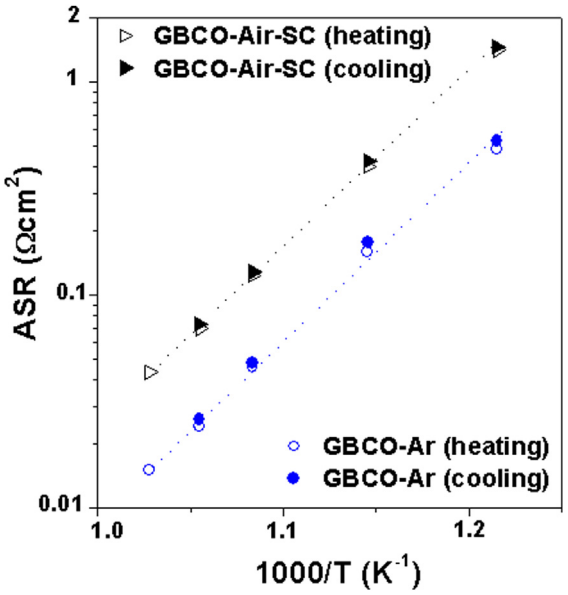

Fig. 10. Arrhenius plot of the area-specific resistance (ASR) values, obtained from the impedance spectra of the GBCO/CGO symmetrical cells.

taking place at intermediate and low frequencies respectively [31,32]. In both cases, Fig. 9a and b, the impedance spectra have been corrected for the electrode area and divided by 2, given the use of the symmetrical cells. In Fig. 9a, the impedance spectra have been shifted to *x*-axis origin for better comparison between GBCO-Air-SC and GBCO-Ar.

Area Specific Resistance values associated to the overall electrode polarization processes of GBCO-Ar and GBCO-Air-SC over CGO electrolytes are shown in Fig. 10 as functions of temperature. The ASR values have been determined from raw impedance spectra taking into the account the high and low-frequency *x*-axis intercepts. Similar ASR values are obtained on both heating and cooling cycles. The electrode performance is better for symmetric cells with $GdBaCo_2O_{5+\delta}$ prepared in Argon atmosphere as electrode in the whole range of temperature. In particular, the ASR of the electrode process decreases from $\approx 0.12\ \Omega\ cm^2$ for GBCO-Air-SC to $\approx 0.04\ \Omega\ cm^2$ for GBCO-Ar at 650 °C. These values are significantly lower than those previously reported for GBCO deposited over CGO electrolytes [3,4]. The experimental analysis of oxygen content and electrode performance seems to indicate that the higher content of oxygen vacancies of the sample prepared in Ar improves the electrochemical reaction at the interface. This is consistent with an ionic-conduction-controlled mechanism as it has been previously suggested [19]. Note that the electronic conductivity remains high enough along the studied conditions for both samples, with values of $\sim 340\ S\ cm^{-1}$ and $\sim 420\ S\ cm^{-1}$ at 650 °C for GBCO-Ar and GBCO-Air-SC, respectively.

Therefore, it seems that the preparation conditions have a strong influence on the oxygen content, crystal structure and electrical and electrochemical properties of $GdBaCo_2O_{5+\delta}$.

4. Conclusions

$GdBaCo_2O_{5+\delta}$ shows a very wide range of oxygen stoichiometry depending on preparation conditions and thermal treatments of the material. The crystal structure is also affected by the oxygen content of the compound. In this sense, layered-type ordering of the Ba and Gd atoms and location of the anion vacancies within the $(GdO)_x$ planes occur with no dependence on the δ value but tetragonal $a_p \times a_p \times 2a_p$ unit cell is observed for the materials with oxygen contents corresponding to $\delta < 0.5$ values and orthorhombic crystal structure is observed for the materials with oxygen contents with $\delta > 0.5$ values. However, there are two different orthorhombic structures, one is pseudotetragonal with $a_p \times b_p \times 2a_p$ unit cell and the other one with $\sqrt{2}a_p \times \sqrt{2}b_p \times 2a_p$ unit cell for the compound with the highest oxygen content and tilting of the CoO_6 octahedra. Formation of domains of the unit cell oriented in perpendicular directions is characteristic of the crystals with orthorhombic structure. A meta-stable superstructure with $a_p \times 3a_p \times 2a_p$ unit cell, probably due to extra ordering of the anion vacancies within the $(GdO)_x$ planes is formed for δ values close to 0.33.

Both oxygen stoichiometry and crystal structure have a high impact on the physical properties of the material. In particular, significantly better electrochemical properties (lower ASR values), which depend on the electrical properties, are observed for the material prepared under Ar gas flow. This fact could be related to the ion conducting properties of the compound and hence, the sample prepared in Ar could have higher ion conductivity than the samples prepared in air due to the higher anion vacancies content. Even the domain formations could influence in some way on the electrochemical properties of the material.

Acknowledgements

S.G.-M., D. M-G. and J.P.-M. thank the Spanish MEC for funding Projects MAT2010-19837-C06-03 and PIB2010JP-00181 and CAM for Project MATERYENER-2 P2009/PPQ-1629 EC.

References

[1] A. Aguadero, L. Fawcett, S. Taub, R. Woolley, K.T. Wu, N. Xu, J.A. Kilner, S.J. Skinner, J. Mater. Sci. 47 (2012) 3925–3948.
[2] E. Kendrick, P.R. Slater, Annu. Rep. Prog. Chem. Sect. A Inorg. Chem. 109 (2013) 396–420.
[3] A. Chang, S.J. Skinner, J.A. Kilner, Solid State Ionics 177 (2006) 2009–2011.
[4] A. Tarancon, S.J. Skinner, R.J. Chater, F. Hernández-Ramírez, J.A. Kilner, J. Mater. Chem. 17 (2007) 3175–3181.
[5] G. Kim, S. Wang, A.J. Jacobson, L. Reimus, P. Brodersen, C.A. Mims, J. Mater. Chem. 17 (2007) 2500–2505.
[6] K. Zhang, L. Ge, R. ran, Z. Shao, S. Liu, Acta Mater. 56 (2008) 4876–4889.
[7] A. Tarancón, M. Burriel, J. Santiso, S.J. Skinner, J.A. Kilner, J. Mater. Chem. 20 (2010) 3799–3813.
[8] A.A. Taskin, A.N. Lavrov, Y. Ando, Appl. Phys. Lett. 86 (2005) 091910.
[9] A.A. Taskin, A.N. Lavrov, Y. Ando, Prog. Solid State Chem. 35 (2007) 481–490.
[10] L. Er-Rakho, C. Michel, P. Lacorre, B. Raveau, J. Solid State Chem. 73 (1998) 531–535.
[11] A. Maignan, C. Martin, D. Pelloquin, N. Nguyen, B. Raveau, J. Solid State Chem. 142 (1999) 247–260.
[12] W.S. Kim, E.O. Chi, H.S. Choi, N.H. Hur, S.J. Oh, H.C. Ri, Solid State Commun. 116 (2000) 609–614.
[13] Y. Moritomo, T. Akimoto, M. Takeo, A. Machida, E. Nishibori, M. Takata, M. Sakata, K. Ohoyama, A. Nakamura, Phys. Rev. B 61 (2000) R13325–R13328.
[14] C. Frontera, J.L. García-Muñoz, A. Llobet, M.A.G. Aranda, Phys. Rev. B 65 (2002), 180405(R)-1–180405-4.
[15] A.A. Taskin, A.N. Lavrov, Y. Ando, Phys. Rev. B 71 (2005) 134414.
[16] N. Ishizawa, T. Asaka, T. Kudo, K. Fukuda, N. Abe, T. Arima, J. Solid State Chem. 198 (2013) 532–541.
[17] A. Yan, M. Yang, Z. Hou, Y. Dong, M. Cheng, J. Power Sources 185 (2008) 76–84.
[18] A. Yan, B. Liu, Y. Dong, Z. Tian, D. Wang, M. Cheng, Appl. Catal. B 80 (2008) 24–31.
[19] A. Tarancón, J. Peña-Martínez, D. Marrero-López, A. Morata, J.C. Ruiz-Morales, P. Núñez, Solid State Ionics 179 (2008) 2372–2378.
[20] D. Parfitt, A. Chroneos, A. Tarancón, J.A. Kilner, J. Mater. Chem. 21 (2011) 2183–2186.
[21] M. Burriel, J. Peña-Martínez, R.J. Chater, S. Fearn, A.V. Berenov, S.J. Skinner, J.A. Kilner, Chem. Mater. 24 (2012) 613–621.
[22] J.C. Pérez Flores, C. Ritter, D. Pérez-Coll, G.C. Mather, F. García-Alvarado, U. Amador, J. Mater. Chem. 21 (2011) 13195–13204.
[23] D. Johnson, ZView: a Software Program for IES Analysis, Version 2.9c, Scribner Associates, Inc., 2005.
[24] D.Y. Woodward, I.M. Reany, Acta Crystallogr. B 61 (2005) 387–399.
[25] A. Morata-Orrantia, S. García-Martín, M.A. Alario-Franco, Chem. Mater. 15 (2003) 363–367.

[26] S. García-Martín, M.A. Alario-Franco, H. Ehrenberg, J. Rodríguez-Carvajal, U. Amador, J. Am. Chem. Soc. 126 (2004) 3587–3596.
[27] A. Tarancón, D. Marrero-López, J. Peña-Martínez, J.C. Ruiz-Morales, P. Núñez, Solid State Ionics 179 (2008) 611–618.
[28] L. Mogni, F. Prado, C. Jiménez, Alberto Caneiro, Solid State Ionics 240 (2013) 19–28.
[29] J. Peña-Martínez, A. Tarancón, D. Marrero-López, J.C. Ruiz-Morales, P. Núñez, Fuel Cells 8 (2008) 351–359.
[30] N. Li, Z. Lü, B. Wei, X. Huang, K. Chen, Y. Zhang, W. Su, J. Alloys Compd. 454 (2008) 274–279.
[31] S.B. Adler, Solid State Ionics 111 (1998) 125–134.
[32] S.B. Adler, Chem. Rev. 104 (2004) 4791–4843.